Numerical Simulation of a PMSM Model Considering Saturation Saliency for Initial Rotor Position Estimation

Ying Yan[1], Jianguo Zhu[1], Youguang Guo[1], Jianxun Jin[2]

1. Faculty of Engineering, University of Technology, Sydney, PO Box 123, Broadway, NSW 2007, Australia
E-mails: yingyan@eng.uts.edu.au, joe@eng.uts.edu.au, youguang@eng.uts.edu.au

2. Center of Applied Superconductivity, University of Electronic Science and Technology of China, Chengdu, China
E-mail: jxjin@uestc.edu.cn

Abstract: With the wide application of permanent magnet synchronous motors (PMSMs), particularly the surface mounted type, the limitations of the conventional PMSM model have become apparent, in which no saturation saliency is incorporated. As a result, the numerical simulation is not applicable for the initial rotor position estimation, which is vital for sensorless motor operation. To avoid the difficulty for developing new initial rotor position estimation techniques through the process of experimental trial and error, a new PMSM model is presented in this paper. The presented model considers both structural and saturation saliencies, enabling fast and cost-effective numerical trial and error for new initial rotor position detection methods. Unlike the constant apparent inductances in the conventional model, the nonlinear self and mutual incremental inductances in the proposed model are expressed by Fourier series and experimentally determined by a specific method to reflect the structural and saturation saliencies, which exist in both salient- and nonsalient-pole PMSMs. Based on the proposed model and the measured inductance patterns, an initial rotor position estimation scheme is numerically simulated and experimentally tested.

Key Words: Permanent magnet synchronous motor (PMSM), PMSM model, numerical simulation, saturation saliency, nonlinear inductance, initial rotor position estimation.

1 INTRODUCTION

In the past decade, the sensorless control of permanent magnet synchronous motors (PMSMs) has attracted a great attention in order to avoid the use of mechanical position sensors, which have various limitations such as the hardware complexity and hence the increased system cost and reduced system reliability [1-3]. Besides many other advantages, such as the simplicity of the control algorithm and fast dynamic response, the direct toque control (DTC) scheme does not need a position sensor at medium and high speeds since it can identify the position of the rotor magnetic flux vector from the back electromotive force (*emf*) [4, 5]. When the rotor is stationary or rotating at low speeds, however, the DTC scheme cannot operate well. For practical application, it is crucial to identify the correct initial rotor position, especially for starting under full load.

To acquire the rotor position information at standstill or low speed, the structural and magnetic saturation saliencies, which exist to a large or small extent in almost all types of PMSMs, are often utilized. In most cases, the position of the rotor axis could be acquired with the structural saliency, while the magnetic polarity could only be identified by using the saturation saliency, which is generated by the rotor permanent magnets and stator currents. The information of the structural and magnetic saturation saliencies can normally be obtained by measuring the stator winding inductances as functions of the rotor position and stator currents [6].

Most of the initial rotor position estimation methods proposed so far can be effective for motors with large structural saliency, e.g. the interior PMSM. However, for the surface mounted PMSM, which does not have significant structural saliency, it is a serious problem to detect the rotor position at zero or low speeds. Many efforts have been made in this field such as high frequency signal injection method [7] and voltage pulse method [8, 9], and the latter is adopted in the work of this paper.

Because of the lack of an appropriate PMSM model that incorporates both structural and saturation saliencies, the major current method for studying the initial rotor position estimation techniques is the experimental trial and error method, which takes a lot of time to implement and is not cost effective. The time-consuming tests can now be overcome by conducting a numerical trial and error process. This task, however, cannot be fulfilled by the conventional model, which incorporates only the structural saliency.

In this paper, a nonlinear model of PMSMs which incorporates both the structural and magnetic saturation saliencies is presented. In this model, the self and mutual incremental inductances of the stator phase windings are expressed by Fourier series as functions of the rotor position and stator currents. A method to measure the incremental inductances on a surface mounted PMSM is outlined. With the model, an initial rotor position estimation scheme using voltage pulses is numerically simulated. The scheme is also tested and the results are compared with the inductance patterns. In this way, the effectiveness of the scheme can be analyzed and evaluated before being implemented in the practical system.

2 NONLINEAR MODEL OF PMSM WITH SALIENCIES

2.1 Flux Linkage and Circuit Equations

In terms of flux linkages and circuit parameters, the voltage equations of the three phase windings can be written as

$$v_j = R_j i_j + \sum_{k=a}^{c} L_{jk} \frac{di_k}{dt} + e_{jf} + e_{j\theta} \quad (j=a, b, c) \qquad (1)$$

where v_j are the phase terminal voltages, R_j the phase winding resistances, $e_{jf}=\omega_r d\psi_{jf}/d\theta$ the emfs induced by the rotor magnets, $\omega_r=d\theta/dt$ is the mechanical angular speed of the rotor, and $e_{j\theta} = \omega_r \sum_{k=a}^{c} (\frac{\partial L_{jk}}{\partial \theta} i_k)$ the phase emfs induced by the variation of flux linkage due to the saliencies.

2.2 Electromagnetic Torque

The electromagnetic torque of the PMSM can be obtained by taking the partial derivative of the system co-energy, W_f', with respect to the rotor position angle θ, i.e. $T=\partial W_f'/\partial\theta$, as:

$$T_{em} = \sum_{j=a}^{c} [i_j \frac{\partial \psi_{jf}}{\partial \theta} + \frac{1}{2} \sum_{k=a}^{c} (\frac{\partial L_{jk}}{\partial \theta} i_j i_k)] \qquad (2)$$

3 INCREMENTAL INDUCTANCE

3.1 Experimental Measurement of Phase Inductances

To measure the self and mutual incremental inductances that incorporate the structural and saturation saliencies, the influence of both the rotor and stator fluxes should be considered. For the rotor flux, the inductances can be measured at different rotor positions, which are related to the structural saliency. Meanwhile, for the stator flux, DC offsets, i_{DC}, with different amplitudes and positions are used to emulate the saturation effect of the 3 phase currents, which corresponds to the saturation saliency.

The experiment was carried out on a 3-phase 6-pole surface mounted PMSM, which is rated as 1000 W, 128 V and 6.5 A. The rotor of the motor is locked by a dividing head. Various DC offsets are injected to one of the stator windings to emulate the effect of stator flux. Meanwhile, a small AC current is applied to one phase while the other two are open-circuited. The self and mutual inductances of phases a, b and c at different rotor positions and stator fluxes can then be calculated via circuit analysis, as shown in Fig. 1.
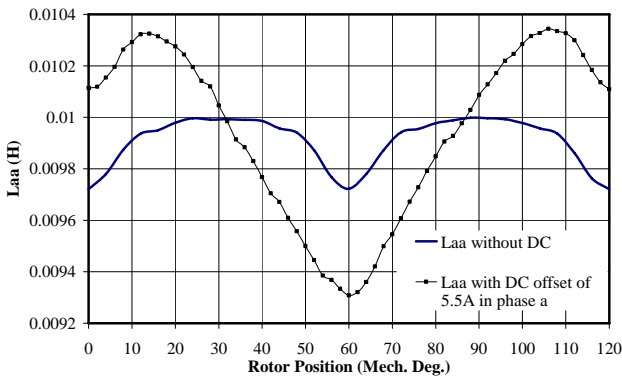
(a)
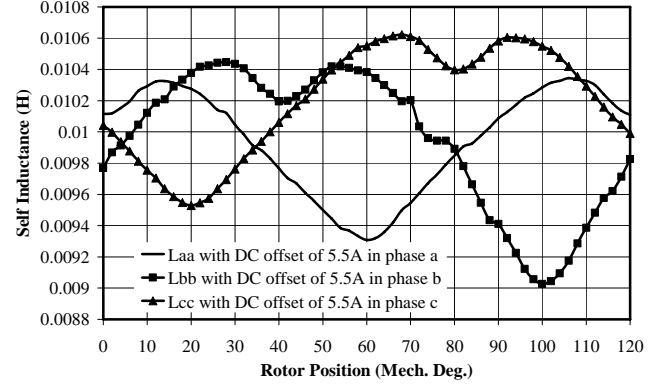
(b)

Fig. 1: (a) L_{aa} at various rotor positions with a DC offset of 5.5A in phase a and without DC offset; (b) Three phase self inductances with a DC offset of 5.5A in the three phase stator windings.

3.2 Analytical Expression of Nonlinear Inductance

Since the flux produced by the rotor permanent magnets of a PMSM can be considered as a constant, the inductances can be expressed as functions of the position of rotor flux, θ_r, the position of the stator flux, θ_s, and the amplitude of stator flux $|\Phi_s|$. From Fig. 1, it can be seen that the self and mutual inductances of the stator windings incorporating the structural and saturation saliencies, and thus a large amount of data are required to describe these functions numerically.

As discussed in [10], the phase inductance can be considered as a periodic function of the rotor angular position and varies nonlinearly with the stator current due to the saturation saliency. In the experiment, DC offsets have been used to emulate the stator flux, and therefore, the inductances can be further expressed as $L(i_{DC}, \theta_r, \theta_{DC})$, where i_{DC} and θ_{DC} refer to the amplitude and position of the applied DC offsets, and θ_r is the rotor position where the measurement is taken. For such a relationship, the following Fourier series with current dependent polynomial coefficients appears to be appropriate:

$$L(i_{ms}, \alpha, \delta) = a_0(i_{ms}, \alpha)$$
$$+ \sum_{m=1}^{n} (a_m(i_{ms}, \alpha) \cos(m\delta) + b_m(i_{ms}, \alpha) \sin(m\delta)) \qquad (3)$$

In Fig. 2, Φ_{s1}, Φ_{s2}, and Φ_{s3} are the stator fluxes generated by the DC offsets in stator windings of phases a, b, and c, respectively, and Φ_r is the rotor flux at a given rotor position. When the DC offset is applied in phase a, as shown in Fig. 2(a) by Φ_{s1} with an arbitrary different rotor position, the measured self inductance of phase a, L_{aa}, corresponds to $\alpha=0°$, $\delta=0°$-360°, and $i_{ms}=0$~I_{rated} (the rated current). Similarly in Figs. 2(b) and (c), L_{aa} corresponds to $\alpha=120°$ and $240°$, $\delta=0°$-360°, and $i_{ms}=0$~I_{rated}, respectively, because of the symmetry of three phase stator windings.

Fig. 3 shows the self inductance of phase a, L_{aa}, at different α with $\delta=0°$-360° and $i_{ms}=5.5$A, and Fig. 4 the mutual inductance between phases b and c, L_{bc}, with a DC offset of 5.5 A at different α.

In this way, the structural and saturation saliencies of the motor magnetic field could be mapped out in terms of the three phase self and mutual inductances, and finally, the

nonlinear expression of the self and mutual inductances at any rotor and stator flux can be readily incorporated into the PMSM model presented in Section 2.
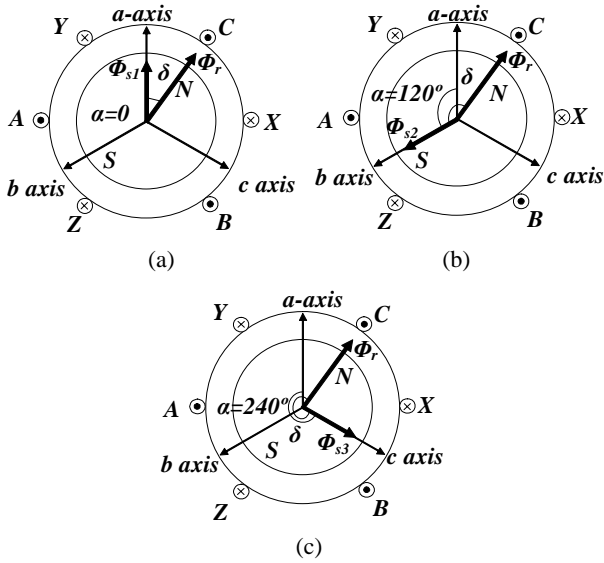

(a)   (b)

(c)

Fig. 2: Illustration of α and δ with a DC offset applied in (a) phase a, (b) phase b, and (c) phase c.
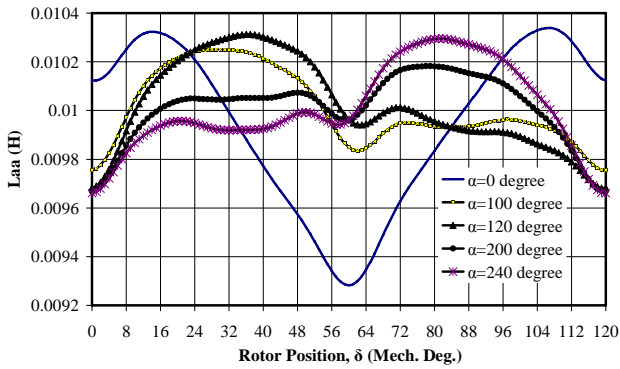
Fig. 3: Measured and computed L_{aa} vs. α with a DC offset of 5.5A
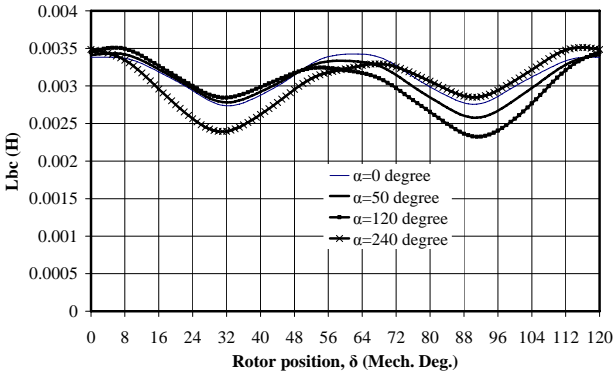

Fig. 4: Measured and computed L_{bc} vs. α with a DC offset of 5.5A

4   INITIAL ROTOR POSITION ESTIMATION

4.1 Principle and System Configuration

As discussed above, the winding inductances are functions of the rotor position and stator currents. With this feature, two kinds of voltage pulses with high and low amplitudes, as shown in Fig. 5, are injected into the stator winding terminals, respectively, for initial rotor position estimation.
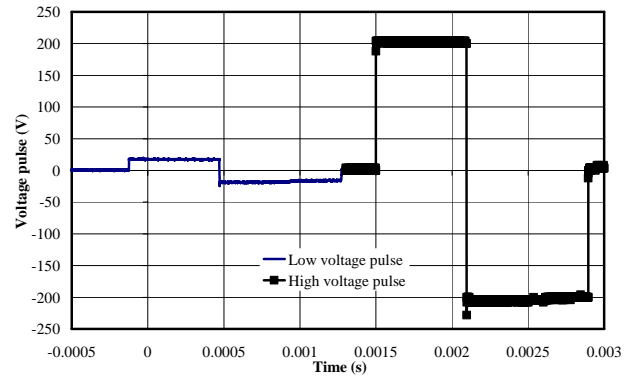

Fig. 5: Low and high voltage pulses

4.2 Experimental Results

Both the high and low voltage pulses were applied to the testing motor. For each phase, the measurement was taken at every locked rotor position and the motor was mechanically rotated from one position to the next. The measured three phase currents with high voltage pulses are plotted in Fig. 6.
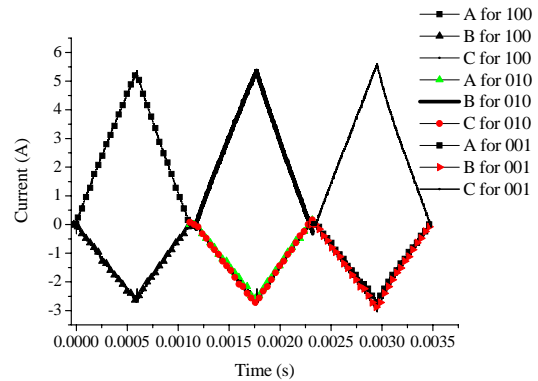

Fig. 6: Experimental current response to high voltage pulse

4.3 Comparison of Peak Current and Inductance

By analyzing the peak current waveform in Fig. 7 under the non-saturated and saturated conditions, it can be seen the magnetic saturation due to the stator currents could be neglected with the low voltage pulse. However, with the high voltage pulse, the magnetic saturation becomes evident.

As demonstrated in Fig. 7(a) by the peak current variation with low voltage pulses and in Fig. 1(a) by the self inductance variation without the DC offset, the structural saliency is very small due to the surface mounted structure of the testing motor, and it is difficult to identify the position of rotor flux from these profiles.

The effect of the saturation saliency becomes sufficiently evident in the profiles of the peak currents with high voltage pulses shown in Fig. 7(b) and the self inductances with a DC offset of 5.5A shown in Fig. 1(b). At some positions, the magnetic circuit becomes more saturated resulting in a smaller stator phase winding inductance when the stator flux produced by the high voltage pulses aids the rotor flux. At positions where the stator and rotor fluxes are opposite, however, the magnetic circuit becomes less saturated and the stator phase winding inductance becomes larger. The clear correspondence between the rotor position and current

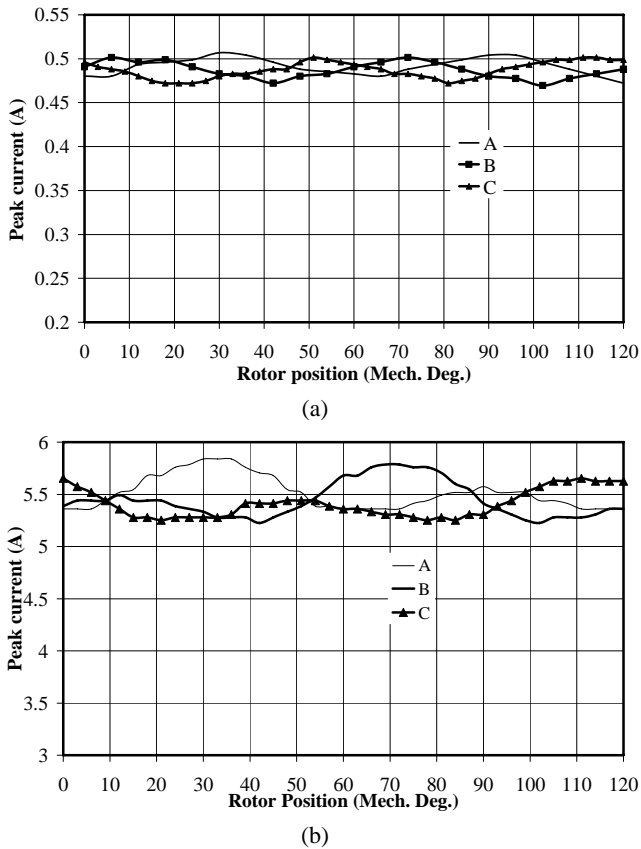and inductance profiles as shown in Fig. 8 provides a possibility to estimate the initial rotor position.

(a)

(b)

Fig. 7: Peak current with (a) low, and (b) high voltage pulse.

For the surface mounted PMSM, since the q-axis inductance is higher than that of the d-axis, the positions of the d- and q-axes can be clearly identified in both profiles of the inductance measured with and without the DC offset shown in Fig. 8. Due to the structural saliency, the peak current profile produced by the high voltage pulses reaches a valley when the stator flux aligns with the q-axis, and a peak when the stator flux aligns with the d-axis. It can be seen that the detected positions of d- and q-axes based on the inductance profile agree with the results based on the peak current variation.

Once the positions of d- and q-axes are determined, the rotor polarity (north or south pole) can be revealed by the inductance profile with DC offsets, in which the saturation saliency is reflected. By comparing the absolute inductance values on the d-axis, the rotor polarity could be identified, e.g. the smaller value corresponds to the N pole.

Meanwhile, the rotor polarity can also be identified by comparing the magnitudes of the peak stator currents on the d-axis. If the stator flux aids the rotor flux (same polarity) on the d-axis, the magnetic circuit becomes more saturated, and thus the magnitude of the stator current produced by the high pulse voltage would be higher than that when the stator flux opposes the rotor flux (opposite polarity) and the magnetic circuit becomes less saturated [2]. As illustrated in Fig. 8, the rotor polarities deduced by both the peak current variation and inductance profiles are the same.
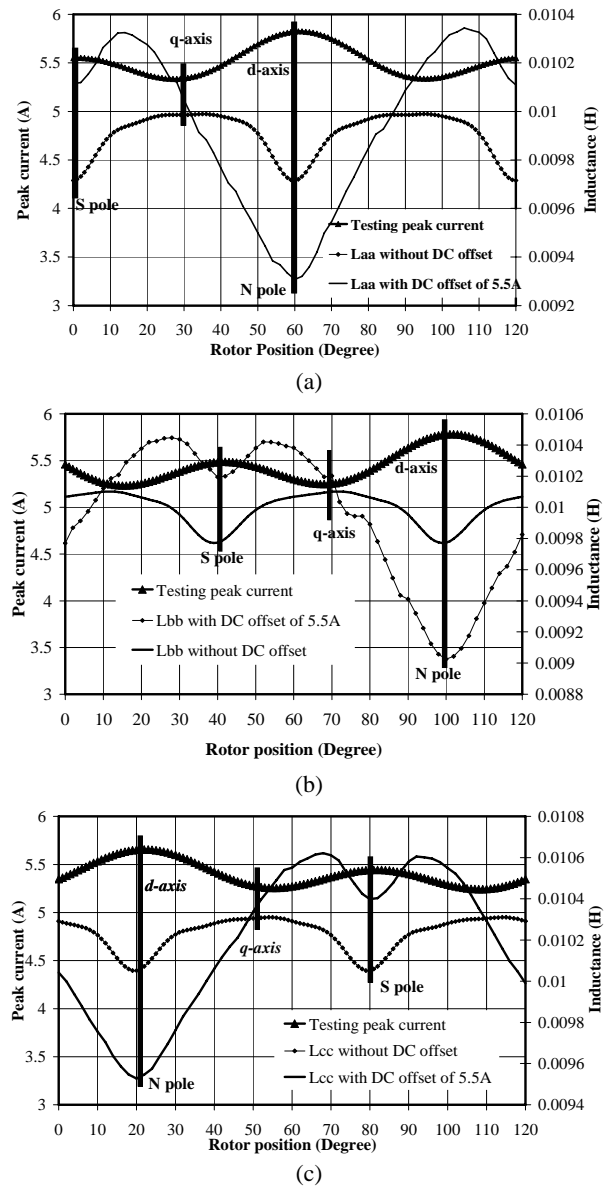

(a)

(b)

(c)

Fig. 8: Correspondence between the variations of inductance and peak current of (a) phase a, (b) phase b, and (c) phase c.

4.4 Simulated and Measured Peak Currents

A Simulink model of the PMSM at standstill has been built and the voltage pulse injection algorithm outlined above is numerically simulated with the measured inductances as the parameters. Fig. 9 plots both the simulated and measured peak currents of phase a versus the rotor position when a high voltage pulse with a magnitude of 148 V and a pulse width of 0.6 ms is applied.

The general profiles of the simulated and experimental peak currents are similar. As mentioned previously, the self and mutual inductances were measured only at limited rotor positions with several number of DC offsets applied in the stator windings, and the linear interpolation was performed to deduce the inductances at arbitrary rotor position and stator magnetic field. This means that the inductance values at these positions may be inaccurate and therefore, some error would appear in the simulated results.
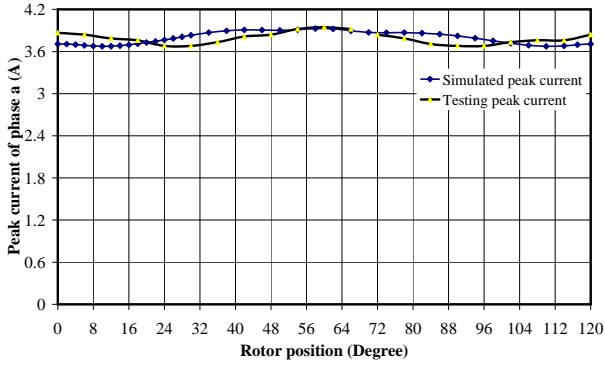
Fig. 9: Simulated and measured peak currents of phase *a*.

4.5 An Algorithm for Detecting Initial Rotor Position

The above analysis shows that the positions of the *d*- and *q*-axes and the rotor polarity could be identified from the measured peak current versus rotor position curve. The peak current with the high voltage pulses can be modeled as [8, 9]

$$I_a = I_0 + \Delta I_{01} \cos\left(\theta_e\right) + \Delta I_{02} \cos\left(2\theta_e\right) \tag{4}$$

$$I_b = I_0 + \Delta I_{01} \cos\left(\theta_e - \frac{2\pi}{3}\right) + \Delta I_{02} \cos\left(2\theta_e + \frac{2\pi}{3}\right) \tag{5}$$

$$I_c = I_0 + \Delta I_{01} \cos\left(\theta_e + \frac{2\pi}{3}\right) + \Delta I_{02} \cos\left(2\theta_e - \frac{2\pi}{3}\right) \tag{6}$$

where I_a, I_b and I_c are the peak currents of stator phases *a*, *b*, and *c*, θ_e is the rotor position in electrical degrees, $I_0 = (I_a + I_b + I_c)/3$, and coefficients ΔI_{01} and ΔI_{02} are determined by curve-fitting the experimental results.

Based on the above discussion, a very simple algorithm is derived for detecting the initial rotor position. The measured peak current variations of phases *a*, *b* and *c* at different rotor positions are stored in the memory of the microprocessor as a look up table. When the rotor is at standstill, the gate signals of 100, 010, and 001 are produced, and the positive high voltage pulses are applied to the three phase stator winding terminals, respectively. The three phase current responses are recorded and the peak values are selected. With the three peak current values, possible rotor positions can be found by solving (4)-(6) using a sectional interpolation method. For phase *a*, the possible rotor positions corresponding to the peak current I_{ap} can be chosen as θ_{a1} θ_{a2}, θ_{a3}, etc., and similarly, for phases *b* and *c*, the possible rotor positions corresponding to I_{bp} and I_{cp} can be obtained as θ_{b1} θ_{b2}, θ_{b3}, θ_{c1} θ_{c2}, θ_{c3}, etc. Among all these possible rotor positions, the real rotor position is given by the common angle obtained of all three phases. Fig. 10 compares the estimated and real rotor positions.

To assess the accuracy of the scheme, an estimation error is defined as

$$Err = \frac{\sqrt{\frac{1}{(N-1)} \sum_{i=1}^{N} \left(\theta_{i\_est} - \theta_{i\_act}\right)^2}}{\max\left\{\theta_{i\_act}\right\}} \tag{7}$$

where *N* is the number of rotor positions, max{ } the function to identify the maximum value in the actual rotor positions, and θ_{i_est} and θ_{i_act} (*i*=1,2,…,*N*) are the estimated and actual rotor positions, respectively. The error of the estimation results calculated by (7) is 3.1%, which is satisfactory for general engineering work.
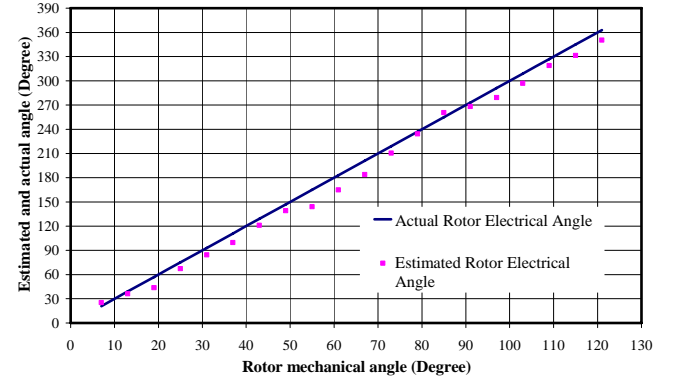

Fig. 10: Estimated and acutal initial rotor positions.

REFERENCES

[1] A. Consoli, S. Musumeci, A. Raciti, and A. Testa. Sensorless vector and speed control of brushless motor drives, IEEE Trans. on Industry Electronics, 1994, 41: 91-95.

[2] S. Ostlund, M. Brokemper. Initial rotor position detections for an integrated PM synchronous motor drive. Proceedings of 30th IEEE Industry Applications Society Annual Meeting[C], 1995: 741-747.

[3] C. French, P. Acarnley. Control of permanent magnet motor drives using a new position estimation technique, IEEE Trans. on Industry Applications, 1996, 32(5): 1089-1097.

[4] L. Tang, M. F. Rahman. A new direct torque control strategy for flux and torque ripple reduction for induction motors drive by using space vector modulation. Proceedings of IEEE Annual Power Electronics Specialists Conference[C], 2001: 1440-1445.

[5] D. Sun, J. G. Zhu, Y. K. He. A space vector modulation direct torque control for permanent magnet synchronous motor drive systems, Proceedings of IEEE International Conference on Power Electronics and Drive Systems[C], 2003: 692-697.

[6] M. Schroedl. Sensorless control of ac machines at low speed and standstill based on the "INFORM" method, Proceedings of 31st IEEE Industry Applications Society Annual Meeting[C], 1996: 270-277.

[7] P. L. Jansen, R. D. Lorenz. Transducerless position and velocity estimation in induction and salient AC machines, IEEE Trans. on Industry Applications[C], 1995, 31(2): 240-247.

[8] P. B. Schmidt, M. L. Gasperi, G. Ray, A. H. Wijenayake. Initial rotor angle detection of a nonsalient pole permanent magnet synchronous machine, Proceedings of 32nd IEEE Industry Applications Society Annual Meeting[C], 1997: 459-463.

[9] P. B. Schmidt. Method and Apparatus for Rotor Angle Detection, U.S. Patent 6 172 498, 2001.

[10] P. Cui, J. G. Zhu, Q. P. Ha, G. P. Hunter, V. S. Ramsden. Simulation of non-linear switched reluctance motor drive with PSIM, Proceedings of 5th International Conference on Electrical Machines and Systems[C], 2001: 1061-1064.